# Creep Properties of Sn-Ag Solder Joints Containing Intermetallic Particles

**S. Choi, J.G. Lee, F. Guo, T.R. Bieler, K.N. Subramanian, and J.P. Lucas**

*The creep behavior of the eutectic tin-silver joints and tin-silver composite solder joints containing 20 vol.% of $Cu_6Sn_5$, $Ni_3Sn_4$, and $FeSn_2$ intermetallic reinforcements introduced by in-situ methods was investigated. These creep tests were carried out using single shear lap solder joints at room temperature, 85°C, and 125°C. The creep resistance was similar in magnitude for all alloys, and with increasing temperature, the stress exponents decreased in a manner consistent with power-law breakdown behavior. The $FeSn_2$ intermetallic reinforced composite solder was found to be the most creep-resistant alloy at room temperature. Creep failure was observed to occur within the solder matrix in all these solder joints. Although a detailed analysis of the processes involved was difficult because of smearing of the features in the fracture surface, there were indications of grain-boundary separation, ductile fracture, and interfacial separation.*

## INTRODUCTION

Global economic and environmental pressures warrant that lead be removed from electronic solders.[1] In addition, performance limitations of tin-lead solders are being exhausted in the electronics industry due to surface-mount technology requirements. In many electronic systems, reliability losses have been found to result mainly from mechanical failures of the solder joints rather than device malfunctions.[2] Several lead-free solders have been considered as alternatives to tin-lead solders, with eutectic tin-silver solder (Sn-3.5Ag in wt.%) emerging as a leading lead-free candidate.[3–6] For electronic systems used in harsh conditions such as automotive under-the-hood and aerospace applications, a composite solder approach has been proposed.[7–9]

In thermomechanical fatigue at high homologous temperatures, both thermal and athermal processes are operative.[3] At high frequencies or low temperatures, failure is dominated by athermal processes. However, at low strain rates or high temperatures, creep deformation dominates. Creep has been identified as a major deformation mode of the solder joint. Grain boundary sliding, an important deformation mechanism in creep, was typically observed in thermomechanically fatigued solder joints.[10]

Creep deformation of the Sn-3.5Ag solder has been investigated.[8,11–16] However, there is no clear agreement about the responsible creep mechanism. Mathew et al.[11] reported that the Sn-3.5Ag bulk solder of 20 μm grain size exhibited the stress exponent of 5 and 60.7 kJ/mol activation energy. They compared this data with the creep data of pure tin of 150 μm grain size with a stress exponent of 7.6 and an activation energy of 60.3 kJ/mol; lattice diffusion-controlled dislocation climb was cited as the controlling mechanism. Despite the difference in stress exponents, creep deformation of Sn-3.5Ag solder was therefore attributed to the same mechanism as that of pure tin. Yang et al.[12] and Liang et al.[13] regarded Sn-3.5Ag solder as a particle-hardened alloy. Dislocation climb over the $Ag_3Sn$ particles was considered as the rate-controlling mechanism.

Darveaux et al.[14] performed creep tests using actual ball-grid arrays of Sn-3.5Ag solder joints. From the measured stress exponent of 5.5, they concluded that dislocation climb was the controlling mechanism. However, the observed activation energy of 38.5 kJ/mol was considerably lower than the expected value of lattice (106 kJ/mol) or dislocation pipe (63 kJ/mol) diffusion in pure tin. They surmised that the activation energy was stress dependent since the data was in the power law breakdown regime, producing a lower activation energy than usual.

Igoshev et al.[15] suggested other mechanisms, such as grain-boundary sliding and/or dislocation movement, to account for observed stress exponents higher than 5. Other microstructural studies on crept specimens appear to support this suggestion.[15,16] Frear[16] reported that the creep strain was accommodated through the tin matrix of 1 μm grain size, at tin-tin grain boundaries. Igoshev et al.[15] observed that microcracks were accumulated at grain boundaries

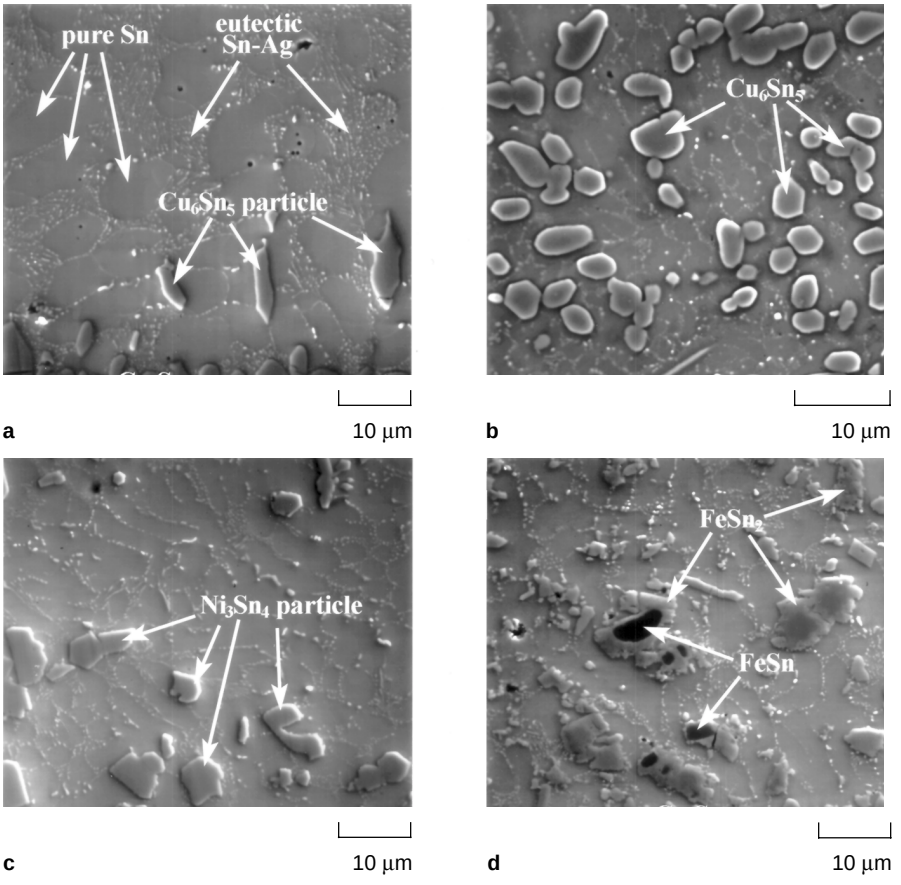


Figure 1. SEM micrographs showing initial microstructure of the solder joint: (a) Eutectic tin-silver solder; (b) $Cu_6Sn_5$ particle-reinforced Sn-3.5Ag solder; (c) $Ni_3Sn_4$ particle-reinforced Sn-3.5Ag solder; and (d) $FeSn_2$ particle-reinforced Sn-3.5Ag solder.

## EXPERIMENTAL PROCEDURES

Sn-3.5Ag solder stock was received in the form of cast ingots. Tin-silver composite solders were prepared by incorporating 20 vol.% $Cu_6Sn_5$, $Ni_3Sn_4$, or $FeSn_2$ intermetallic particles into the Sn-3.5Ag solder by in-situ methods. The composite solders were made by intrinsically producing the intermetallic reinforcements within the solder, rather than by mechanically adding intermetallic particles to the solder. The Sn-3.5Ag and composite solders were rolled to produce a sheet of about 100 μm thick and cut into preforms of about 1.0 $mm^2$ area. Single shear lap joints with an area of about 1 $mm^2$ were fabricated with preforms of the solders by soldering together two copper substrates of semi-dog bone shape. Further experimental details about fabrication of the solder joint can be found elsewhere.[17] The solder joints were prepared for microstructural examination by standard metallographic techniques, finishing with 0.05 μm $SiO_2$ colloidal suspension.

Constant load creep tests were performed by hanging a dead-load on one side of the single shear lap solder joint mounted on an aluminum beam. Tests were conducted in air at room temperature, 85°C, and 125°C, with the applied stress varying from 3 MPa to 25 MPa. Figure A shows how a test specimen was set up for elevated temperature creep experiments. Such testing was carried out using a small heating pad affixed to the side of the copper substrate, which was electrically connected to a variable transformer. The temperature was measured by a thermocouple soldered closely to the joined region of the copper substrates.

Creep strain was measured using laser ablation patterns placed on the side of the solder joint by an excimer laser before creep testing.[18] Optical microscopic images of laser patterns were taken periodically. The creep strain was determined by calculating the changes in slope of the laser patterns, which distort from the original position with time. Details of creep-data analysis using this method were described in the previous study.[19]

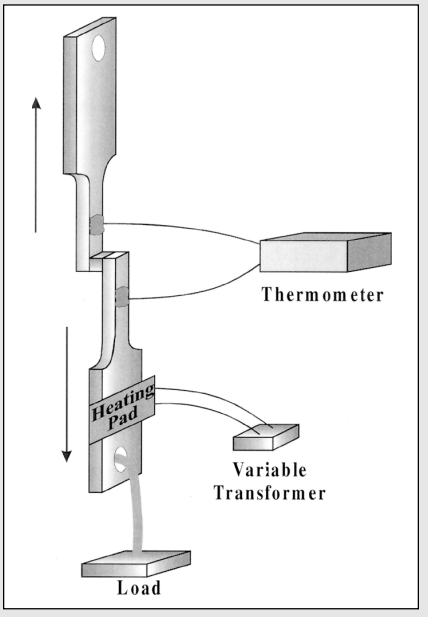


Figure A. A schematic drawing of creep testing method.

The fracture surfaces of the solder joints were examined by scanning-electron microscopy after the solder joints failed. The actual stress applied to the solder joint was determined by dividing the applied load by the actual joined area, obtained after subtracting the large void area in a solder joint cut by the fracture plane.

due to grain-boundary sliding, leading to an intergranular fracture. The accumulation of grain-boundary defects started at an earlier stage of creep and lasted for at least 70-80% of the lifetime.

In a previous study,[8] Sn-3.5Ag solder joints reinforced with $Cu_6Sn_5$ particles showed two or three order of magnitude higher creep resistance in as-fabricated condition, compared to the eutectic tin-silver solder joint. But with aging, the difference in creep resistance was less dramatic. In this study, the creep deformations of unaged Sn-3.5Ag solder and its in-situ composite solders reinforced with $Cu_6Sn_5$, $Ni_3Sn_4$, or $FeSn_2$ are characterized by constant-load creep testing of single shear lap solder joints.

## RESULTS AND DISCUSSION

### Initial Microstructure

The microstructure of a eutectic tin-silver solder joint in Figure 1a shows the copper substrate, continuous $Cu_6Sn_5$ interfacial layer, and eutectic tin-silver solder matrix. The eutectic tin-silver solder matrix consisted of almost pure tin grains peppered with $Ag_3Sn$ particles. Within the solder matrix, a few $Cu_6Sn_5$ intermetallic particles were observed near the copper substrate, which were formed during reflow of the solder joint.[20]

Particulate-reinforced Sn-3.5Ag composite solder joints (Figures 1b–d), showed a microstructure similar to that of the eutectic tin-silver solder joint along with incorporated $Cu_6Sn_5$, $Ni_3Sn_4$, and $FeSn_2$ particles, respectively. The solder joint reinforced with $FeSn_2$ particles revealed that some $FeSn_2$ possessed a dual composition manifested by the difference in contrast, indicating two different intermetallics of FeSn (dark contrast) and $FeSn_2$ (bright contrast). There were variations in the particle shape and size distribution in each composite solder joint.

### Creep Properties of Solder Joints

Figure 2 shows the variation of secondary creep strain-rate with applied stress at various temperatures for eutectic Tin-silver solder joints and its composite solder joints. A power law relationship of the form $\dot{\gamma} = A\tau^n$ describes the data over the stress ranges and temperatures used in this study, with some scatter in the data. $\dot{\gamma}$ is the shear strain-rate, $\tau$ and n are the shear stress and stress exponent, and A is a constant. The stress exponents tended to decrease with increasing temperature with exception of the $Cu_6Sn_5$ particulate-reinforced solder joint, which exhibited a stress exponent of 6.5 at 85°C. The stress exponents at a given temperature were found to be more or less

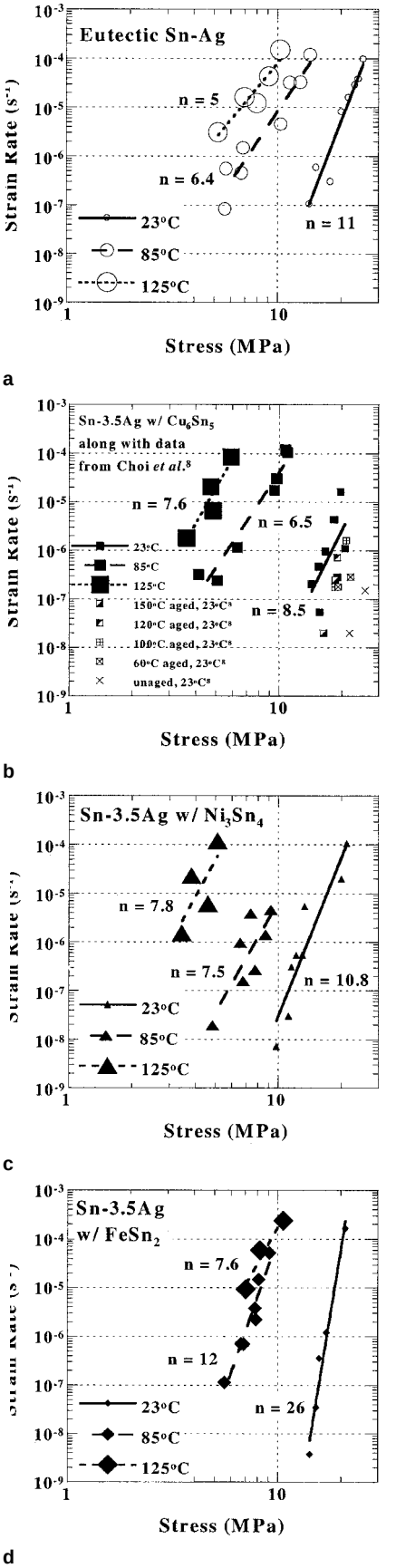


Figure 2. Steady state strain-rate vs. applied stress: (a) Eutectic tin-silver solder joints, (b) $Cu_6Sn_5$ composite solder joints along with data from Choi et al.,[8] (c) $Ni_3Sn_4$ composite solder joints, and (d) $FeSn_2$ composite solder joints.

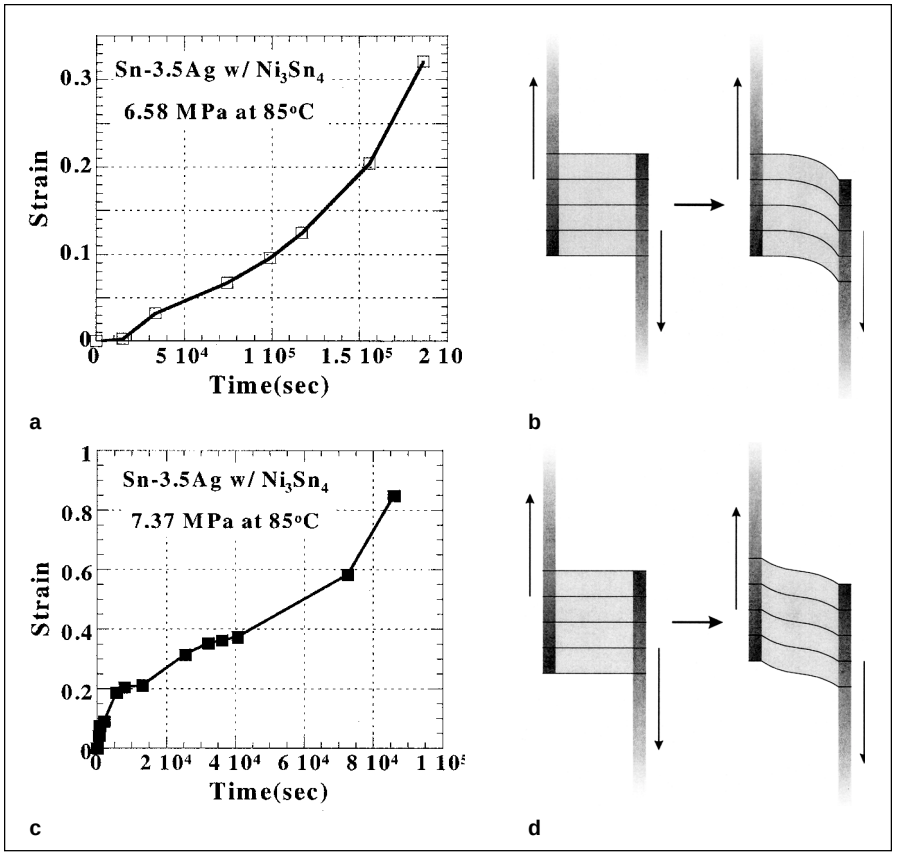


Figure 3. Two representative creep curves and schematic diagrams illustrating different damage accumulation across the solder joint. Inhomogeneous deformation are depicted in (a) and (b), while (c) and (d) represent homogeneous deformation.

similar, ranging from 5 to 12, which are similar to values given in other studies.[12,13] The solder joint reinforced with $FeSn_2$ particles showed the highest stress exponent values at room temperature.

Data from our prior work[8] on the same $Cu_6Sn_5$ composite solder joints shows substantially better creep resistance than the present study, as indicated in Figure 2b. The datum points for the earlier study were obtained by unloading the specimen periodically to take micrographs of a particular scratch to quantify the shear displacement, allowing recovery that was not possible in the present study, where loading was uninterrupted. This implies that when the loading direction was reversed, recovery effects apparently reduced the mobile dislocation density that could be regenerated upon reloading, reducing strain over time by 2–3 orders of magnitude. When these joints were aged, the creep resistance was degraded due to the effects of coarsening the $Ag_3Sn$ particles.

The scatter in data was related to differences in how damage accumulation developed during creep deformation. Figure 3 shows two representative creep curves of strain vs. time along with schematic diagrams of damage accumulation in the solder joint during creep deformation for the $Ni_3Sn_4$ particle-reinforced solder joint crept at 85°C. The creep curve in Figure 3a shows an upward curvature for most of its lifetime, resulting in a lower creep strain before fracture, whereas the creep curve in Figure 3c exhibits the conventional downward curvature expected in the materials where dislocation climb is the controlling mechanism. The difference between the two curves correlates with the different deformation history of the solder joint. The solder joint that exhibited an upward curvature in creep curve had inhomogeneous strain distribution across the joint thickness, resulting from preferential strain on one side of the solder joint as shown in Figure 3b. On the other hand, the solder joint shown in Figure 3d, exhibiting a downward curvature in creep curve, deformed nearly uniformly across the joint thickness. The inhomogeneous deformation in Figure 3b is thought to be influenced by undetected defects present initially in the solder joint, such as porosity or a non-uniform particle distribution produced during specimen fabrication. In many cases, inhomogeneously deforming joints also showed higher minimum creep rates than specimens with more homogeneous deformation. This result points out that a better microstructural control is required to obtain consistent benefits from particle-reinforced composite solders.

Figure 4 compares the behavior of each composite solder joint with the eutectic solder joint, and the data of Darveaux and Banerji[14] using a Dorn model for creep, which is most valid at lower normalized stresses below $\tau/G \sim 7 \times 10^{-4}$, where power-law breakdown is not apparent.

$$\dot{\gamma} = A\frac{DGb}{kT}\left(\frac{\tau}{G}\right)^n\left(\frac{b}{d}\right)^p \quad \text{or} \quad \frac{\gamma T}{A'G}\exp\left(\frac{+Q}{kT}\right) = \left(\frac{\tau}{G}\right)^n$$

where D is the operative diffusion process for creep with activation energy Q, G is the temperature-dependent shear modulus, b is the Burgers vector, k is Boltzmann's constant, T is temperature in K, d is the grain size, n is the stress exponent, taken to be 5.5 (as used by Darveaux and Banerji), p is the grain size exponent, and A is a geometrical parameter representing microstructural features. When terms that are assumed to be constant are combined into A', a set of data could be plotted using the second equation with various values of Q. The value of Q that causes the data at different temperatures to collapse onto a single line represents a good estimate of the controlling activation energy for creep. For the eutectic solder joints, a value of 60 kJ/mol caused a better fit of the data than the value of 38.5 kJ/mol used by Darveaux and Banerji. Sixty kJ/mol is about half of the activation energy for tin self-diffusion,[11,14] suggesting that grain boundary or pipe diffusion may control deformation of the eutectic solder joints. A value of Q = 120 kJ/mol was most effective for the $Cu_6Sn_5$ and

$Ni_3Sn_4$ composite solder joints, but for the $FeSn_2$ composite solder joints, Q = 38.5 kJ/mol was more effective than 60 kJ/mol or 120 kJ/mol. Once Q was determined, the A' parameter could be found so that the solder joints could be compared uniformly. These values are indicated in the plots in Figure 4.

Figures 4a–c show how the composite solder joints typically have the same properties as the eutectic solder joints at elevated temperatures, but not at lower temperatures. For the $Cu_6Sn_5$ and $Ni_3Sn_4$ composite solder joints, room-temperature deformation appears weaker than the eutectic solder joints at equivalent normalized stresses, while the $FeSn_2$ composite solder joints are effectively stronger. This suggests that the Dorn model may be meaningful at high temperatures, but a different composite modeling strategy needs to be developed for composite solder joints at lower temperatures.

The morphology of the reinforcement particles differs among the three composite solders. $Cu_6Sn_5$ particles tend to be elliptical, $Ni_3Sn_4$ particles are angular, and $FeSn_2$ particles tend to be rounded, although they exhibit irregular interface morphology. These variations imply that the mechanisms of dislocation climb over particles would be different for the three reinforcements due to different interface chemistry, geometry, and interfacial dislocation structure, and this may account for the difference in stress exponents. Since solder microstructure is very sensitive to thermomechanical history, the variation in creep behavior may be attributed to the variation in microstructure.

### Fracture of Solder Joints

A representative fracture surface of the crept solder in Figure 5a illustrates the presence of porosities in the solder joint. The porosity within the solder joints ranged from 5% to 30% of the total joint area. The large-scale porosity was subtracted in calculation of the actual stress applied on the solder joint since voids do not carry the load. Figure 5b shows the typical fracture surface of a solder joint crept to failure in shear. Most of the fracture surface exhibited failure by shear through the solder matrix. Thus, the fracture surface shown in Figure 5b illustrates the smeared tin phase in the shearing direction.

In the minor areas of the fracture surface, fracture processes that included tensile as well as shear components of deformation were found. Eutectic tin-silver solder joints exhibited cracks along the grain boundaries of the tin phase as shown in Figure 6a, indicating that the creep strain was accommodated by intergranular separation. Spherical and elliptical dimples of tin phase illustrated in Figure 6b were found in the fracture surface of $Ni_3Sn_4$ particle-reinforced solder joint crept at room temperature, indicating that this region failed in a highly ductile manner. A particle can be found at the bottom of some dimples, indicating cavity nucleation at the particle/matrix interface. Similar dimples were observed in the fracture surface of the $Cu_6Sn_5$ particle-reinforced solder joints crept at room temperature.

Fracture by interfacial separation between the $Cu_6Sn_5$ intermetallic interfacial layer and the solder matrix was found in very few regions. Figures 6c–d show the faceted surface of the $Cu_6Sn_5$ intermetallic layer in the fracture surface of the eutectic tin-silver solder joint crept at 85°C and 125°C. The exposure of the $Cu_6Sn_5$ intermetallic interfacial layer in the fracture surface indicates that the crack grew locally by debonding between the $Cu_6Sn_5$ intermetallic layer and solder matrix. The fracture surface region in Figure 6c shows complete debonding, but Figure 6d shows remaining solder ligaments, indicating partial debonding. It is possible that if the solder joint fracture surface were not smeared

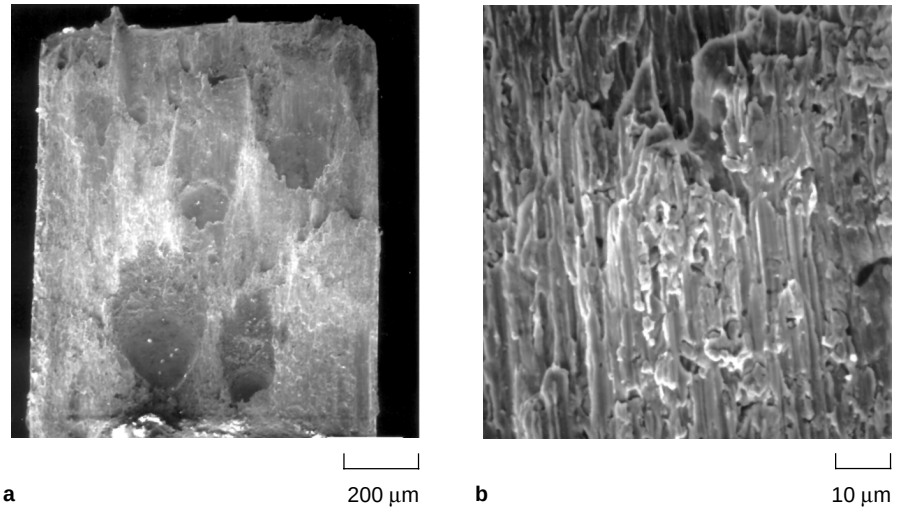


a b

Figure 5. Representative fracture surface of the crept solder joint: (a)A $Cu_6Sn_5$ particle-reinforced Sn-3.5Ag solder joint with 10.5% porosity, and (b) smeared surface due to fracture in pure shear.

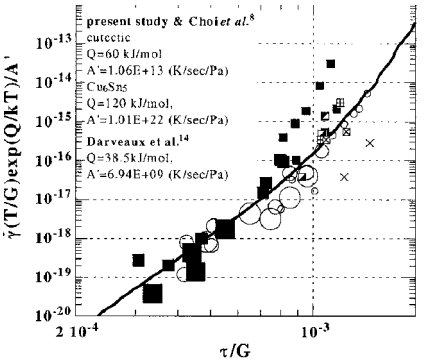


a

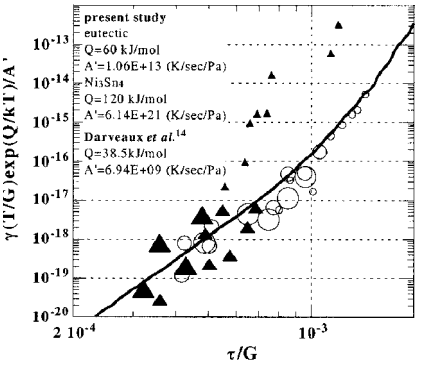


b

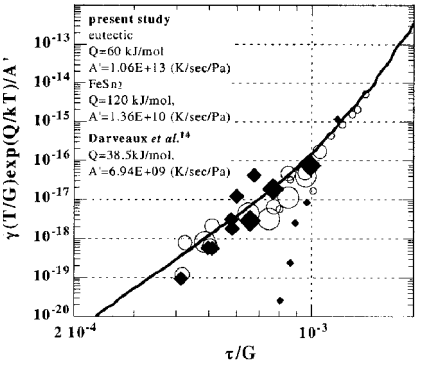


c

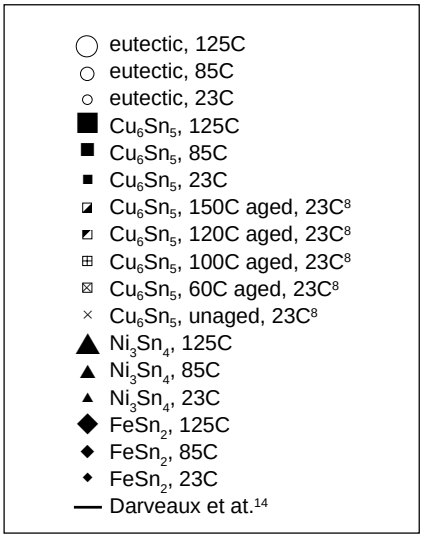


Figure 4. The normalized steady state behavior of eutectic tin-silver and composite solder joints along with data of Darveaux and Banerji's:[14] (a) Eutectic and $Cu_6Sn_5$ composite solder joints; (b) eutectic and $Ni_3Sn_4$ composite solder joints; and (c) eutectic and $FeSn_2$ composite solder joints.

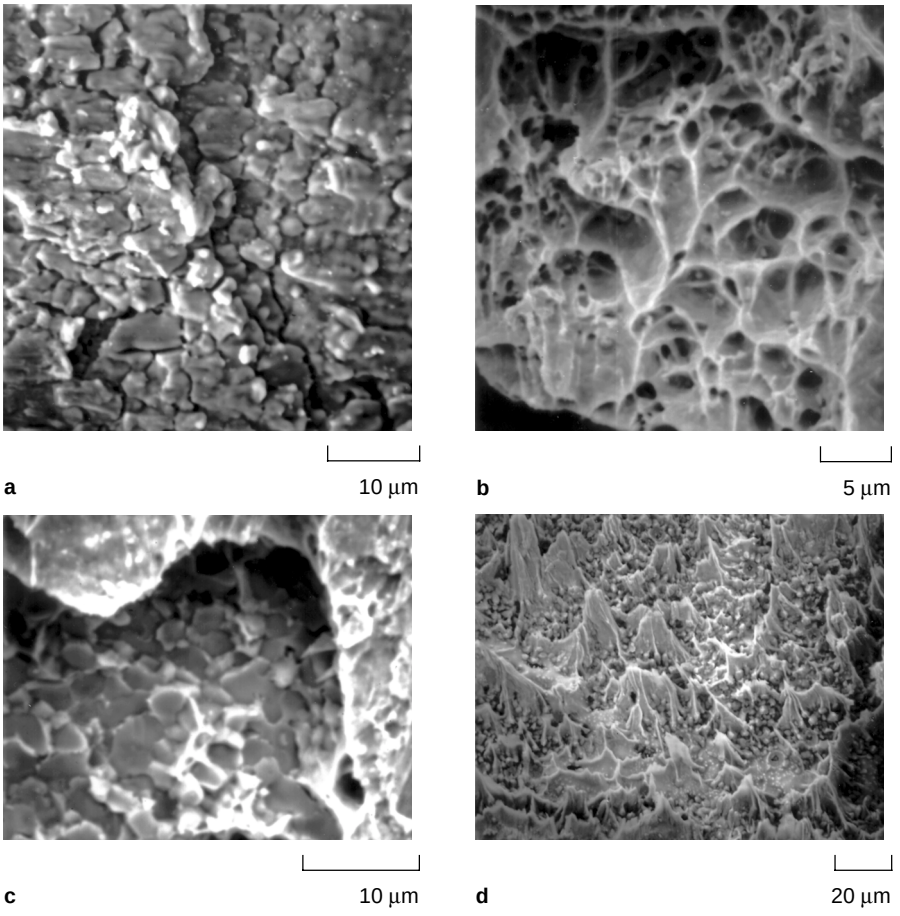


Figure 6. SEM micrographs showing fracture processes: (a) Cracks developed along tin-tin grain boundaries; (b) dimples indicating ductile fracture; (c) complete debonding of $Cu_6Sn_5$ interfacial layer and solder matrix; and (d) partial debonding.

by shear during fracture, the favored fracture processes could be observed. However, it is not easy to ascertain which is the preferred fracture process based on the complications indicated. If the overall failure process were a mixture of shear and tension, these failure modes would probably dominate the fracture surface more than the smearing shown in Figure 5b. The initiation of a crack may develop by local tensile effects that are evident in Figure 6.

## ACKNOWLEDGEMENT

*The authors would like to thank Composite Materials and Structure Center at Michigan State University for providing financial support for this study. They also thank the National Science Foundation for support under contract NSF-DMR-0081796.*

## References

1. B.P. Richards et al., *Lead-Free Soldering* (London: U.K. Department of Trade and Industry, 1999).
2. P.T. Vianco and D.R. Frear, *JOM*, 45 (7) (1993), p. 14.
3. H. Mavoori et al., *J. Electron. Mater.*, 26 (7) (1997), p. 783.
4. S. Chadaet al., *Soldering & Surface Mount Technology* (26) (July 9, 1997).
5. M. McCormack and S. Jin, *1994 IEEE/CPMT Int. Electronics Manufacturing Technology Symposium* (Piscataway, NJ: IEEE, 1994), p. 7.
6. W. Yang, L.E. Felton, and R.W. Messler, Jr., *J. Electron. Mater.*, 24 (10) (1995), p. 1465.
7. A.W. Gibson et al., *Design & Reliability of Solders and Solder Interconnections,* ed. R.K. Mahidhara et al. (Warrendale, PA: TMS, 1997), p. 97.
8. S.L. Choi et al., *Design & Reliability of Solders and Solder Interconnections,* ed. R.K. Mahidhara et al. (Warrendale, PA: TMS, 1997), p. 241.
9. A.W. Gibson et al., *IEEE 5th International Symposium on Electronics and the Environment* (Piscataway, NJ: IEEE, 1997), p. 246.
10. S. Choi et al., *J. Electron. Mater.*, 2 (10) (2000), p. 1249.
11. M.D. Mathew, S. Movva, and K.L. Murty, *Key Engineering Materials*, 171-174 (2000), p. 655.
12. H. Yang et al., *1996 46th Electronic Components and Technology Conference* (Piscataway, NJ: IEEE, 1996), p. 1136.
13. J. Liang et al., *Mater. Res. Soc. Symp. Proc.*, Vol. 445 (Warrendale, PA: MRS, 1997), p. 307.
14. R. Darveaux and K. Banerji, *1992 42nd Electronic Components and Technology Conference* (Piscataway, NJ: IEEE, 1992), p. 538.
15. V.I. Igoshev et al., *J. Electron. Mater.*, 27 (12) (1998), p. 1367.
16. D.R. Frear, *JOM*, 48 (5) (1996), p. 49.
17. S. Choi et al., *J. Electron. Mater.*, 28 (11) (1999), p. 1209.
18. J.P Lucas et al., *J. Electron. Mater.*, 28 (11) (1999), p. 1268.
19. J. McDougall et al., *Mater. Sci. Eng.*, A285 (2000), p. 25.
20. H.D. Blair et al., *1996 IEEE/CPMT Int. Electron. Manuf. Technol. Symp.* (Piscataway, NJ: IEEE, 1996), p. 282.
21. V.I. Igoshev and J.I. Kleiman, *J. Electron. Mater.*, 29 (2) (2000), p. 244.

*S. Choi, J.G. Lee, F. Guo, T.R. Bieler, K.N. Subramanian, and J.P. Lucas are with the Department of Materials Science & Mechanics at Michigan State University.*

**For more information, contact K.N. Subramanian, Michigan State University, Department of Materials Science and Mechanics, 3536 Engineering Building, East Lansing, Michigan 48824-1226; (517) 353-5397; fax (517) 353-9842; e-mail subraman@egr.msu.edu.**